Preparation of sulfonated coal@ZVI@chitosan-acrylic acid composite and study of its removal of groundwater Cr(VI)

Jianlei Gao
Zhengzhou University
Mengyuan Feng
Zhengzhou University
Yixin Yan (yxyan@zzu.edu.cn)
Zhengzhou University https://orcid.org/0000-0002-2330-6550
Zixu Zhao
Zhengzhou University
Yingchun Wang
Zhengzhou University

Research Article

Keywords: sulfonated coal, Chitosan-acrylic acid sol, Zero-valent iron,Chromium

Posted Date: June 6th, 2022

DOI: https://doi.org/10.21203/rs.3.rs-1603008/v1

Preparation of sulfonated coal@ZVI@chitosan-acrylic acid composite and study of its removal of groundwater Cr(VI)

Jianlei Gao, Mengyuan Feng, Yixin Yan ✉, Zixu Zhao, Yingchun Wang

School of Ecology and Environmental Science, Zhengzhou University, 100 Kexue Avenue, Zhengzhou, Henan 450000, PR China

✉ Corresponding author. Tel: +86 13676931078; E-mail address: yxyan@zzu.edu.cn

Abstract

The effects of Cr(VI) pollution in groundwater run wide and deep. Without effective remediation, Cr(VI) harms the environment and human health. With in situ treatment methods in which permeable reactive walls serve as the main body, chitosan-acrylic acid sols (CS-AA) were used to stabilize zero-valent iron (ZVI), and acid-modified sulfonated coal (SC) was used as the carrier to prepare SC@ZVI@CS-AA. The interaction between SC@ZVI@CS-AA and Cr(VI) conformed to a pseudo second-order kinetic model suggesting chemisorption. The Langmuir model provided a good fit to the data for adsorption of Cr(VI) by SC@ZVI@CS-AA. SC@ZVI@CS-AA was characterized using XRD, FTIR, SEM and TG−DSC analyses. The effects of contact time, initial Cr(VI) concentration, temperature, material ratios, pH, dosage of SC@ZVI@CS-AA and interfering ions on the adsorption of Cr(VI) were investigated. Under the optimal conditions, the efficiency for removal of Cr(VI) reached 98.5%. The adsorption of Cr(VI) was significantly inhibited by SO_4^{2-} . In addition, the capacity for adsorption of Cr(VI) by SC@ZVI@CS-AA remained above 70% after three use cycles.

Overall, SC@ZVI@CS-AA proved to be a promising and environmentally friendly medium for removal of Cr(VI) from groundwater.

Keywords: sulfonated coal; Chitosan-acrylic acid sol; Zero-valent iron; Chromium

Introduction

Pollution with the heavy metal chromium originates from wastewater and slag produced by electroplating, tanning, metallurgy, mining, chemical production, etc. If the area in which chromium pollution was generated is not protected, solid waste comprising chromium slag and other chromium-containing hazardous materials will leach chromium-containing compounds into soil and water under the influence of the external environment. Cr(VI) in groundwater pollutants has high solubility and mobility, which makes its pollution range wide and deep(Jobby et al., 2018), and it can seriously damage the ecological environment and endanger human health.

Permeable wall reaction technology (PRB) emerged in the 1990s as an in situ method for treating groundwater contamination(Hedin et al., 1994), and it has received widespread attention because of its wide remediation and control range, low cost, and low energy consumption(Obiri-Nyarko et al., 2014; Liu et al., 2015). Active materials are very important for Cr(VI) removal from groundwater, since the PRB technology should support quick reactions with Cr(VI), avoid producing secondary pollution and exhibit good stability, permeability and economy(Bronstein, 2005).

In recent years, scholars have performed considerable research on PRB fillers, among which zero-valent iron (ZVI) is commonly used as a reaction medium(Wilkin et al., 2010); it was also reported that ZVI can be applied in practical engineering(Henderson and Demond, 2007). ZVI has the advantages of high reaction rates, large specific surface areas, and ample reducing capability. However, ZVI is

46 prone to agglomeration, loss and instability in practical applications, which leads to
47 blockage of PRB systems(A et al., 2010). Numerous studies have shown that
48 modification of ZVI by using cellulose, chitosan, polyacrylic acid and zeolite as
49 stabilizers retains the advantages of ZVI and overcomes the disadvantages of ZVI, such
50 as instability and loss(Tasharrofi et al., 2020, Guan et al., 2019).

51 Chitosan (CS) contains a large number of reactive amino ($-NH_2$) and hydroxy
52 ($-OH$) groups, which can chelate heavy metals and support ion exchange(Wu et al.,
53 2001). CS can be used as a modified coating for metal particles to prevent
54 aggregation(Zhiya et al., 2007; Akg and Mg, 2005); moreover, it has the advantages of
55 low price, biodegradability, and nontoxicity(Guibal, 2004), making it a promising
56 environmental material. Geng et al(Geng et al., 2009). used CS as a stabilizer for
57 modifying ZVI and found that ZVI stabilized by CS removed 148.08 mg of chromium
58 per gram, a level that was approximately three times higher than that of unmodified
59 ZVI. More importantly, CS-stabilized ZVI exhibited antioxidant properties and good
60 dispersion. However, the application of natural CS is limited in a practical sense due to
61 its sensitivity to pH and poor mechanical stability in acidic media(Lei et al., 2016). To
62 overcome these limitations, chemical modification of CS is needed(B et al., 2013).
63 Among various modification methods, grafting copolymerization of CS with acrylic
64 acid (AA) further improves the functionality of chitosan(Tao et al., 2003; Lu., 2019)
65 grafted CS with AA and compared the capacities of modified CS and unmodified CS
66 for adsorption of Pb^{+}, Cd^{2+} and Cu^{2+} in water. CS grafted onto AA showed better

67 performance than CS alone for adsorption of all three ions, and the surface of grafted
68 CS exhibited a network structure in which the number of $-NH_2$ groups was
69 approximately doubled. Therefore, CS grafted onto AA can be used to stabilize ZVI
70 and serve as an active PRB material for in situ remediation of groundwater Cr(VI).

71 In PRB remediation of groundwater polluted by Cr(VI), the reaction medium must
72 have good adsorption and reducing properties in addition to permeability. Therefore,
73 porous materials have been considered potential solid carriers for loading CS-stabilized
74 ZVI and forming a composite medium, which would improve the permeability of the
75 reaction medium(Belhaj et al., 2015). The porous carrier materials commonly used in
76 remediation of heavy metals in water bodies include activated carbon, attapulgite,
77 bentonite, etc. The activity of activated carbon gradually decreases during the
78 remediation process, and the material is expensive(Obiri-Nyarko et al., 2014).
79 Attapulgite and bentonite are clay minerals with low permeability, so they are not
80 favored for PRB technology(Pourcq et al., 2015). Sulfonated coal is the product
81 obtained from the interaction of coal with fuming sulfuric acid or concentrated sulfuric
82 acid(Ni., 1997), it is rich in functional groups such as $-OH$，$-NH_2$ and $-SO_3H$ (Jamil
83 et al., 2017), it contains porous structures, and it is an inexpensive and valuable resource.
84 Acid modification of sulfonated coal removes soluble metal oxides from inner pore
85 surfaces and further opens the pores(Zheng., 2008). Therefore, sulfonated coal can be
86 used as a solid carrier for ZVI stabilized by modified CS to prepare a new PRB active
87 material for removal of chromium.

In this study, a SC@ZVI@CS-AA composite medium was prepared by using biocompatible CS containing ample $-NH_2$ and $-OH$ groups to improve the chemical stability and adsorption capacity of ZVI, and sulfonated coal particles rich in functional groups were used as a support. The surface morphology, structural composition, surface chemical properties and thermal stability were analyzed by SEM, XRD, FTIR and TG−DSC. The effects of different factors, such as material proportions, pH, reaction time (t), initial concentration of Cr(VI) (C_0), adsorbent dosage, reaction temperature (T) and interfering ions, on the adsorption performance of Cr(VI) are discussed. Finally, the mechanism for adsorptive removal of Cr(VI) was analyzed based on the adsorption kinetics and a thermodynamic model. This study provides a reference for the preparation of reaction media used in remediation of Cr(VI)-contaminated groundwater with PRB technology.

Materials and methods

Materials

Chitosan (CS) and sodium tripolyphosphate (TPP) (1%, m/m) were purchased from Aladdin Biochemical Technology Co., Ltd., Shanghai, China. Potassium dichromate (K_2CrO_7) was purchased from Fengchuan Chemical Reagent Co., Ltd., Tianjin, China. Sulfonated coal (1−1.5 mm) is an environmental filter material and was purchased from Hanbang Sewage Treatment Co., Ltd.. Epichlorohydrin (ECH), sodium sulfide and absolute ethanol were purchased from Damao Chemical Reagent Co., Ltd., Tianjin, China. Concentrated sulfuric acid (H_2SO_4) and concentrated nitric acid (HNO_3)

were purchased from Haohua Chemical Reagent Co., Ltd., Luoyang, China. ZVI, acrylic acid (AA), glacial acetic acid and sodium hydroxide (NaOH) were purchased from Mie European Chemical Reagent Co., Ltd., Tianjin, China. All drugs used in these experiments were analytically pure.

Preparation of the SC@ZVI@CS-AA composite

Acid modification of sulfonated coal

Sulfonated coal with particle sizes of 0.5 mm to 1.0 mm was cleaned by deionized water with a solid-liquid ratio of 1 to 30 until the supernatant was clear and no suspended matter was present. The clean sulfonated coal was filtered, spread evenly in an ordinary oven, and dried at 60°C for 12 h(Zhan et al., 2017).

Diluted nitric acid (HNO_3, 2 mol/L) was slowly poured onto dried sulfonated coal and the solid−liquid ratio was kept at 1 to 10. After stirring at 1500 r/min for 24 h, the sulfonated coal was filtered and washed to neutrality with deionized water until the supernatant was clear and no suspended matter was present. Then, the clean sulfonated coal was filtered again and dried at 60°C for 12 h. Sulfonated coal modified by HNO_3 (SC) was obtained.

Preparation of the SC@ZVI@CS-AA composite

CS (1 g) was dissolved in 50 mL of glacial acetic acid (2%, v/v) to form a solution of chitosan with a mass concentration of 2% (Chen et al., 2006)and stirred for 2 h to dissolve it fully and form a transparent, yellowish colloid. Next, 1 mL of AA was added to the colloid for graft modification and stirred at a speed of 1500 r/min for 2 h to obtain

the modified chitosan colloid (CS-AA).

SC (0.2 g) was added to CS-AA and stirred at 1500 r/min for 2 h. Then, 0.05 mL of epichlorohydrin (CS:ECH=2:1(m:v)) was added to the CS-AA as a cross-linking agent(Mei et al., 2019), and stirring was continued for 3 h. Then, 0.07 g of ZVI was mixed and dispersed for 1 h with nitrogen. At the same time, 0.01 mL of sodium tripolyphosphate (CS:TPP = 10:1(m:v)) (Chen et al., 2003)was added to the solution, and then 2 mol/L NaOH was added until no new precipitate was formed. After the system was closed and aged for 24 h, it was washed with deionized water until the washings were neutral. The clean material was dried at 60°C for 12 h in a vacuum oven and ground to obtain the SC@ZVI@CS-AA composite. The basic preparation flow chart is shown in Fig. 1.

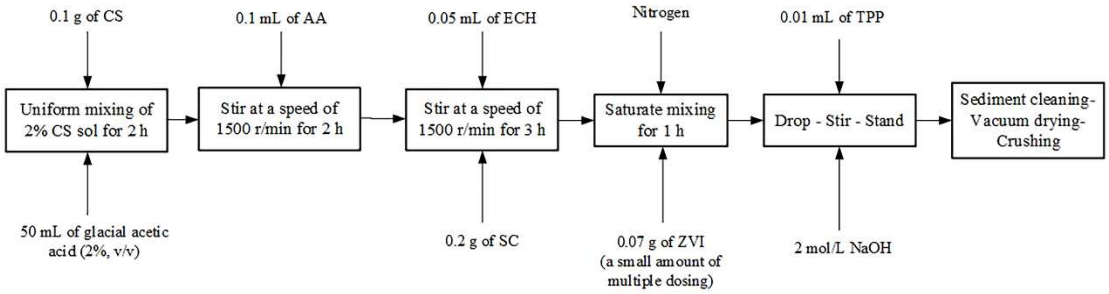

Fig. 1 Basic flow chart for preparation of SC@ZVI@CS-AA

Characterization

The surface morphologies of SC and SC@ZVI@CS-AA were observed by scanning electron microscopy (ZEISS GEMINI 300) at an acceleration voltage of 3 KV, working distance of 5 mm, and multiple scanning with 500 to 20000 scans. The crystal structures of SC and SC@ZVI@CS-AA were analyzed by X-ray diffraction (BRUKER

148 D8 Advance) with a scanning 2θ range of 5 to 90° and a scan step of 0.02456º. The
149 distributions of surface functional groups on SC and SC@ZVI@CS-AA were analyzed
150 by Fourier transform infrared spectroscopy (Thermo Nicolet 6700) at wavelengths
151 between 400 and 4000 cm^{-1} . The thermal stability and composition of SC and
152 SC@ZVI@CS-AA were analyzed by a synchronous thermal analyzer over a
153 temperature range of 30 to 1000°C with a heating rate of 10°C /min.

154 **Adsorption of Cr(VI) by the SC@ZVI@CS-AA composite**

155 A K_2CrO_7 solution with a concentration of 1000 mg/L [measured as Cr(VI)] was
156 prepared as a stock solution. During the batch adsorption experiments, the stock
157 solution of Cr(VI) was diluted to the required concentration, and HNO_3 (0.1 mol/L) was
158 added to adjust the pH. A total of 10 mL of diluted Cr(VI) stock solution was placed
159 into a polyethylene tube (50 mL), and SC@ZV@CS-AA was added to the solution.
160 Then, the solution was placed on a thermostatic oscillator and oscillated at a speed of
161 120 r/min. At a predetermined time, a syringe (20 mL) was used to sample the mixtures
162 in the reaction bottles. After filtration through a membrane (0.45 μm), the concentration
163 of residual Cr(VI) in the solution was determined by diphenylcarbazide
164 spectrophotometry (GB/T 7467-1987, 2003). Determination of total chromium (Total
165 Cr) contrAA700 continuous light source atomic spectrometer, based on linear fitting to
166 calculate its concentration.

167 The adsorption capacity (q_e , mg/g) and removal efficiency (%) of SC@ZVI@CS-
168 AA for chromium were calculated by Equations (1) and (2)

169 $$q_e = \frac{(C_0 - C_e)V}{m} \quad (1)$$

170 $$Removal\ efficiency = \frac{C_0 - C_e}{C_0} \times 100\% \quad (2)$$

171 Where C_0 (mg/L) is the initial concentration of chromium, C_e (mg/L) is the
172 equilibrium concentration of chromium, *m* (g) is the dosage of adsorbent, and *V* (L) is
173 the total volume of solution.

174 To describe the mechanism for adsorption of chromium and the associated rate of
175 reaction, the experimental data were fitted to pseudo first-order, pseudo second-order,
176 and intraparticle diffusion models.

177 The pseudo first-order kinetic model is described by Equation (3)(Lu et al., 2014):

178 $$log(q_e - q_t) = log\ q_e - \frac{K_1}{2.303} t \quad (3)$$

179 The pseudo second-order kinetic model is given by Equation (4)(Divya et al.,
180 2008):

181 $$\frac{t}{q_t} = \frac{1}{K_2 q_e^{\ 2}} + \frac{1}{q_e} t \quad (4)$$

182 The intraparticle diffusion model is described by Equation (5)(Araújo et al., 2017):

183 $$q_t = K_P t^{0.5} + C \quad (5)$$

184 Where q_e (mg/g) is the adsorption capacity of SC@ZV@CS-AA at equilibrium;
185 q_t (mg/g) is the adsorption capacity of SC@ZV@CS-AA at time t; K_1 (min^{-1}), K_2
186 (g/mg·min), and K_d (g/mg·min) are the rate constants for the pseudo first-order, pseudo
187 second-order, and intraparticle diffusion models, respectively; and *C* (mg/g) is the

188 intercept.

189 As the adsorption process reached equilibrium at a certain temperature, the
190 relationship between adsorbate and adsorbent could be assessed with various adsorption
191 isotherm models(Hameed et al., 2007). To analyze the adsorption process, Langmuir,
192 Freundlich and Tempkin isothermal adsorption models were used to simulate the
193 adsorption results.

194 The Langmuir isotherm model assumes that monolayer adsorption occurs on a
195 homogeneous adsorbent surface(Wang et al., 2016). The Langmuir isotherm equation
196 is described by Equation (6):

197 $$\frac{C_e}{q_e} = \frac{1}{q_m K_L} + \frac{C_e}{q_m} \quad (6)$$

198 The Freundlich isotherm model is an empirical model for heterogeneous systems
199 exhibiting multilayer adsorption. The Freundlich isotherm model is expressed by
200 Equations (7) and (8)[M.A. et al., 2019; Zhao. et al., 2011]:

201 $$lg\, q_e = lg\, K_F + \frac{1}{n} lg\, C_e \quad (7)$$

202 $$q_e = \frac{(C_0 - C_e)V}{m} \quad (8)$$

203 The Tempkin isotherm model assumes that the heat of adsorption for supported
204 substrates undergoes a linear decrease(Hu et al., 2011). The Tempkin isotherm model
205 is expressed by Equations (9) and (10):

206 $$q_e = B_T\, ln\, K_T + B_T\, ln\, C_e \quad (9)$$

207 $$B_T = \frac{RT}{b_T} \quad (10)$$

Where q_e (mg/g) is the amount of Cr(VI) adsorbed at equilibrium per unit weight of SC@ZVI@CS; q_m (mg/g) is the maximum adsorption capacity; C_e (mg/L) is the equilibrium concentration of Cr(VI); C_0 (mg/L) is the initial concentration of Cr(VI); K_L (L/mg) is a Langmuir constant; V (L) is the total volume of solution; m (g) is the dosage of adsorbent; K_F ([mg/g][L/mg]$^{-1/n}$) and n are empirical constants for Freundlich adsorption capacity and strength, respectively; R = 8.314 J/(mol K) is the ideal gas constant; T (K) is the absolute temperature; K_T (L/g) is the equilibrium binding constant; B_T (J/mol) is a Tempkin constant; and b_T (J/mol) is the Tempkin constant related to heat of adsorption.

Thermodynamic parameters include the enthalpy change (ΔH^θ), entropy change (ΔS^θ)and Gibbs free energy change (ΔG^θ), which are evaluated by Equations (11), (12) and (13)(Aksu, 2002); these parameters are helpful in further understanding the energy changes occurring in the adsorption process and predicting the adsorption mechanism more effectively.

$$K_d = \frac{q_e}{C_e} \qquad (11)$$

$$ln\, K_d = \frac{\Delta S^\theta}{R} - \frac{\Delta H^\theta}{RT} \quad (12)$$

Where K_d (L/g) is the thermodynamic equilibrium constant; q_e (mg/g) is the amount of Cr(VI) adsorbed at equilibrium per unit weight of SC@ZVI@CS; C_e (mg/L) is the equilibrium concentration of Cr(VI); R = 8.314 J/(mol K) is the ideal gas constant; T (K) is the absolute temperature. plots are made with $1/T$ as the abscissa and $ln\left(q_e/C_e\right)$

as the ordinate, and ΔS^{θ}、ΔH^{θ} are calculated from the intercept and slope. The Gibbs free energy is given by Equation (13):

$$\Delta G^{\theta} = \Delta H^{\theta} - \Delta S^{\theta} T \quad (13)$$

Experiments on adsorption kinetics and isotherms

To study the adsorption kinetics and the influence of reaction time on chromium adsorption, the Cr(VI) stock solution was diluted to three different concentrations (200, 300 and 400 mg/L), and the pH was adjusted to 3. Ten milliliters of solution was added to a polyethylene tube (50 mL) with 0.008 g of SC@ZVI@CS-AA. The reaction was carried out on a constant temperature oscillator with a rotating speed of 120 r/min and a temperature of 25°C. The concentrations of Cr(VI) in the samples were measured at different times (10, 20, 30, 45, 60, 90, 120, 180, 240, 300, 360 and 480 min). Three parallel experiments were used for each determination.

To explore the effects of temperature and initial chromium concentration on the chromium adsorption process, temperatures of 25°C, 35°C, or 45°C were used. The Cr(VI) stock solution was diluted to eight different concentrations (10, 20, 50, 100, 200, 300, 400 and 500 mg/L), and the pH was adjusted to 3. Ten milliliters of solution at each concentration was added to a polyethylene tube (50 mL) with 0.008 g of SC@ZVI@CS-AA. After reaction at 120 r/min for 5 h at the chosen temperature, samples were taken to determine the concentration of Cr(VI) in the solution. Three parallel samples were used for each experiment.

Effects of composite ratio of materials, pH, dosage and coexisting ions

To study the effects of the material composition on the adsorption of Cr(VI), 0.3, 0.5, 1, and .2 g of CS were dissolved into each of four different amounts (15, 25, 50 and 100 mL) of glacial acetic acid (2%, v/v) to give a chitosan solution with a 2% mass fraction(Chen et al., 2006). Based on the CS-AA sol preparation method described above, the corresponding volume of AA was added to obtain four CS-AA samples with different CS contents. Then, 0.2 g of SC was added to each of four CS-AA samples to establish four different mass ratios SC:CS (6:1, 4:1, 2:1, and 1:1). SC@ZVI@CS-AA was prepared with the mass ratio of SC to ZVI unchanged. SC@ZVI@CS-AA was used for adsorption experiments with the following conditions: pH = 3, T = 25°C, and C_0 = 200 mg/L. The optimal dosage of chitosan was determined according to the experimental results. The CS-AA sol was prepared with the optimal amount of chitosan. Five CS-AA sols with the same volume were added to 2 g of SC. Then, five SC@ZV@CS-AA samples with different SC:ZVI mass ratios (8:1, 6:1, 3:1, 1.5:1, 1:1) were prepared by adding ZVI for adsorption experiments. Three parallel samples were used for each experiment.

The effect of pH on the adsorption of Cr(VI) (10 mL, 200 mg/L) was studied with pH values ranging from 3 to 8.5, an adsorbent dose of 0.008 g, a 5 h reaction time, and a reaction temperature of 298 K. To explore the effect of adsorbent dosage on adsorption performance (200 mg/L), the pH was set to 3. Then, varying amounts of SC@ZVI@CS-AA (0.004, 0.008, 0.012, 0.016, 0.02, 0.025 and 0.03 g/L) were added and the

adsorption experiments were carried out at 25°C for 5 h; To study the effects of coexisting ions in water on the adsorption of Cr(VI) (10 mL, 200 mg/L), 0.01 mol of eight electrolytes (NaCl, $CaCl_2$, $MgCl_2$, Na_2SO_4, $NaNO_3$, NaH_2PO_4, $Cd(NO_3)_2 \cdot 4H_2O$) were added to the Cr(VI) solutions containing 0.008 g/L of SC@ZVI@CS-AA, and reactions were carried out at 25°C for 5 h. Three parallel samples were used for each experiment.

Cyclic adsorption experiments with Cr(VI)

To explore cyclic adsorptions with the adsorbent, adsorption experiments were carried out with an initial Cr(VI) concentration of 200 mg/L, adsorbent dosage of 0.008 g/L, temperature of 25°C, pH of 3 and reaction time of 5 h. NaOH (50 mL, 0.1 mol/L) was added to the SC@ZVI@CS-AA, which was filtered out after reaching adsorption saturation, and then the mixed liquor was desorbed in a constant temperature shaker at 25°C for 6 h. The SC@ZVI@CS-AA was filtered again and rinsed to neutral with deionized water, and the adsorption experiment was continued after vacuum drying. This sequence was repeated three times. The concentrations of Cr(VI) and Total Cr in the desorption solution and adsorbed solution were determined. Desorption efficiency (%) is expressed by Equation (14):

$$Desorption\ efficiency = \frac{C_1 \times V_1}{C_0 \times V_0} \times 100\% \quad (14)$$

Where C_1 (mg/L) is the concentration of Cr(VI) in the desorption solution; V_1 (mL) is the volume of desorption solution; C_0 (mg/L) is the initial concentration of

289 Cr(VI) (mg/L); and V_0 (mL) is the volume of the Cr(VI) solution.

290 **Results and discussion**

291 **Characterization**

292 **SEM results**

293 The SEM results for SC and SC@ZVI@CS-AA are shown in Fig. 2. From Fig. 2a,
294 it can be seen that the surface of SC was relatively rough; it showed a lamellar structure
295 with small holes and longitudinal cracks, which provided a large number of support
296 sites for the stable ZVI loaded on CS-AA. In addition, this morphology would hinder
297 the agglomeration of ZVI. As shown in Fig. 2b, the surface of SC@ZVI@CS-AA
298 constituted a continuous mesh structure with abundant small and large pores, which
299 indicated that the modified ZVI (particle sizes of approximately 0.1 – 0.2 μm) was
300 uniformly distributed on the surface of sulfonated coal. This increased the dispersion
301 and stability of ZVI and facilitated full contact between ZVI and Cr(VI), which
302 provided abundant sites for reduction and adsorption and the efficient removal of
303 Cr(VI).

304 **XRD results**

305 Fig. 2c shows the XRD patterns for SC and SC@ZVI@CS-AA. The sharp
306 characteristic peak ($2\theta = 26.9°$) for silicon dioxide (SiO_2) appeared in the diffraction
307 pattern of SC, since the SC used in the experiment was mixed with impurities such as
308 sediment during production. In contrast, the characteristic peak for SiO_2 in the

diffraction pattern of SC@ZVI@CS-AA was weak and broad, which may be due to refinement of the grains or the introduction of chitosan in the modification reaction. In addition, this indirectly indicated the synthesis of new substances on the surface of SC. The peaks for SC@ZVI@CS-AA showed evidence for the (110) crystalline face of body−centered cubic α−Fe ($2\theta = 44.9°$) and a diffusion diffraction peak for the (211) face ($2\theta = 82.6°$) appeared, indicating that ZVI stabilized by CS-AA was successfully loaded onto the SC(Jin et al., 2018).

FTIR results

FTIR results for SC and SC@ZVI@CS-AA are shown in Fig. 2c. Changes in the functional groups on the surface of the material after loading were limited, which was related to the rich content of chemical groups ($-OH$，$-NH_2$ and $-SO_3H$) in sulfonated coal itself. For both SC and SC@ZVI@CS-AA, the peaks at 2919 cm^{-1} and 2870 cm^{-1} showed weak C−H stretching vibrations, and the peak at 1085 cm^{-1} was assigned to a C−C bending vibration. Compared with SC, the absorption peak at 3447 cm^{-1} for SC@ZVI@CS-AA was broadened slightly, which may be due to the introduction of chitosan and increases in the number of O−H and N−H groups on the surface of the material that resulted in an increase in the number of hydrogen bonds(Lei et al., 2020). The peaks at 1625 cm^{-1} were due to C=C stretching vibrations, and the C=C band of SC@ZVI@CS-AA became stronger because of the AA used in the modification process(Pbv et al., 2011). Compared with SC, the FTIR results for SC@ZVI@CS-AA suggested that the peaks at 1321 cm^{-1} were due to C−N stretching

vibrations and the obvious overlapping peaks representing bending vibrations of C−H(Wu., 2002). The above results indicated that the functional groups of AA and CS were introduced on the surface of SC@ZVI@CS-AA and provided coordination for the removal of Cr(VI) and enhanced the binding of Cr(VI) with the modified materials. In addition, the SC solid carrier did not cause changes in the chemical groups carried by the loaded materials.

TG−DSC results

Fig. 2e and f shows TG−DSC curves for SC and SC@ZVI@CS-AA. Fig. 2e shows that the weight lost by SC was approximately 5% at temperatures ranging from 30°C to 600°C, indicating the superior thermal stability of CS. Fig. 2f shows that the weight loss of SC@ZVI@CS-AA was mainly divided into three stages. The first stage occurred between 30°C and 120°C and was due to incomplete drying of free water or crystalline water in the modified material(Hadi et al., 2013), and the weight loss for SC@ZVI@CS-AA was approximately 2%. In the second stage, a weight loss of 9% was observed between 280°C and 320°C. In this stage, the rate of weight loss was fast, and the DSC curve showed a small peak. Because the decomposition temperature of chitosan reached 280°C, polymers of CS were thermally decomposed and produced volatile gases and organic substances. The third stage occurred between 320°C and 600°C. Overall, the weight loss of SC@ZVI@CS-AA was 14% in the range 280°C to 320°C. Considering the weight lost by SC, it was speculated that the carbon-containing polymer loaded on SC@ZVI@CS-AA accounted for approximately 10.7% of the

weight of the material itself. This indicated that the SC carrier could be decomposed at a high temperature, and SC@ZVI@CS-AA maintained good thermal stability at temperatures below 280°C.

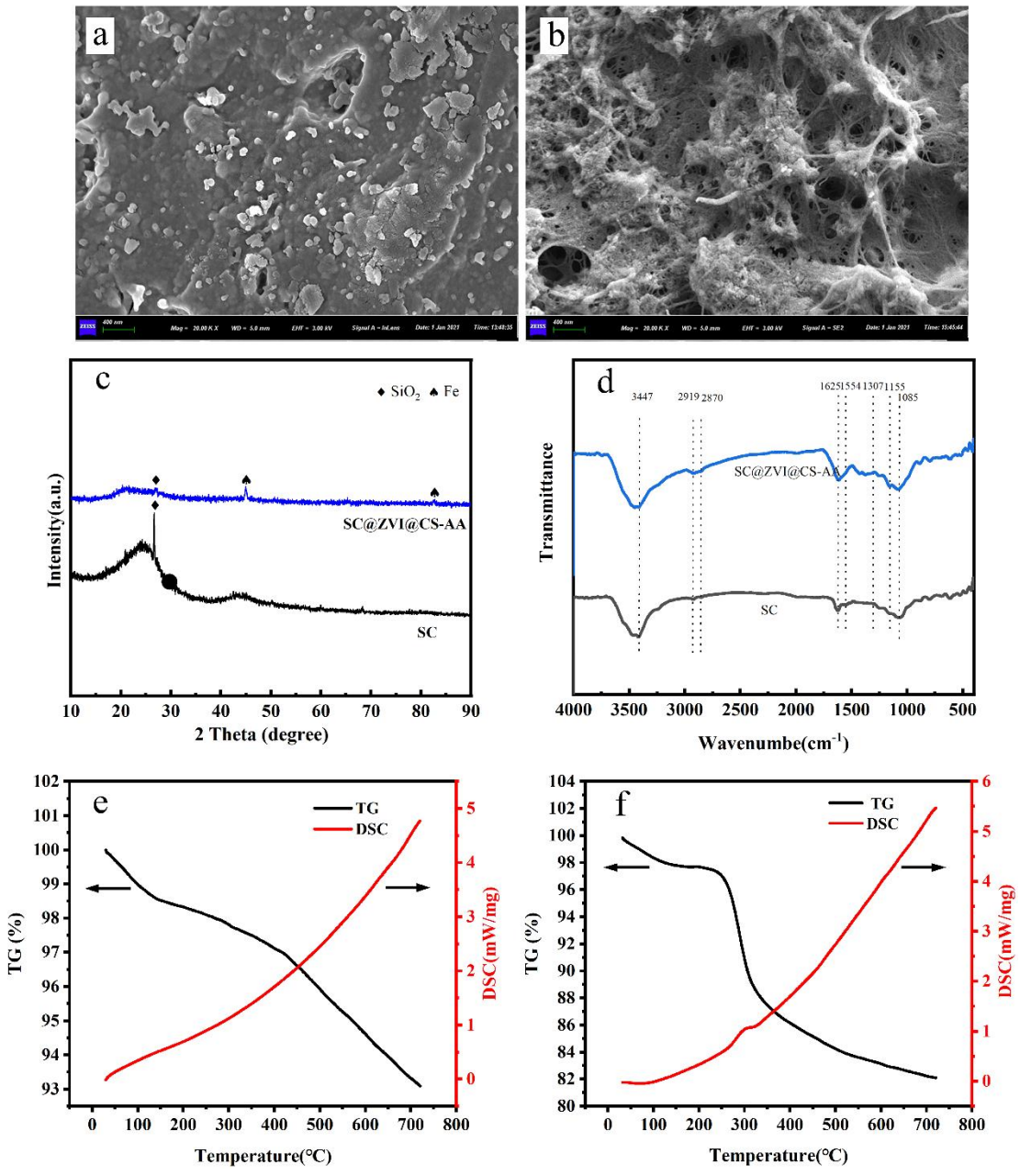

Fig. 2 The characterization of SC and SC@ZVI@CS-AA: (a) SEM results for SC (20 KX magnification); (b) SEM results for SC@ZVI@CS-AA (20 KX magnification); (c) XRD results for

SC and SC@ZVI@CS-AA; (d) FTIR results for SC and SC@ZVI@CS-AA; (e) TG−DSC results of SC; and (f) TG−DSC results of SC@ZVI@CS-AA

Experimental results for batch adsorption of Cr(VI)

Studies of adsorption kinetics

The effect of contact time on adsorption at three different initial Cr(VI) concentrations (200, 300 and 400 mg/L) is shown in Fig. 3a. The q_e of Cr(VI) gradually increased with increasing reaction time. Most of the adsorption process occurred within the first 240 min. With the various initial concentrations (200, 300 and 400 mg/L), the adsorption capacities reached 140.392, 150.544 and 165.148 mg/g within 240 min, respectively. The adsorption capacities increased by only 3.606, 3.377 and 3.236 mg/g between 240 min to 480 min, respectively.

There were a large number of unreacted adsorption sites on the surface of SC@ZVI@CS-AA during the primary stage of adsorption. With a decrease in available adsorption sites, the capacities for adsorption of Cr(VI) increased slowly. Although the chemical groups (−OH, −COOH, and $-NH_2$) carried by SC@ZVI@CS-AA chelated Cr(III) and Fe(III) to promote a reduction reaction(Neto et al., 2019), a small portion of Cr(III) complexed with Fe(III) to form coprecipitated $Fe_xCr_{1-x}OOH$ or $Fe_xCr_{1-x}(OH)_3$ deposited on the surface of ZVI, which hindered electron transfer between ZVI and Cr(VI) and prevented adsorption of Cr(VI) on SC@ZVI@CS-AA(Gong et al., 2016).

The results of treatments with pseudo first-order and pseudo second-order models are shown in Fig. 3b and Fig. 3c, respectively, and the related parameters are shown in

Table S1. According to the fitting curves and correlation coefficients, the pseudo second-order kinetic model (Fig. 3c) was most consistent with the experimental values, while the pseudo first-order model (Fig. 3b) did not fully describe adsorption by SC@ZVI@CS-AA. In addition, the correlation coefficient (R^2) for the pseudo second-order kinetic model was higher than those for other models; moreover, q_e values (149.47, 158.98 and 174.21 mg/L) calculated with the pseudo second-order model were very close to the experimental values. Additionally, they increased with increasing concentration, indicating that the pseudo second-order kinetic model was more suited for explaining the adsorption mechanism; that is, the adsorption rate was controlled by the chemical adsorption stage(Wang et al., 2019).

The curves for the intraparticle model and the related parameters are shown in Fig. 3d and Table S2, respectively. Fig. 3c shows that three-segment linear simulations were carried out at the two inflection points of $t^{0.5}$, which indicated a multilinear response corresponding to three stages of rapid external diffusion and adsorption, internal surface and pore diffusion, and gradual approach to equilibrium. The rate for adsorption of Cr(VI) from the liquid phase to the surface of SC@ZVI@CS-AA was higher than that for the pores because of the higher value of K_p for the first stage of the process. By observing the value of the boundary layer effect (C), it was found that the C value for the third stage was significantly higher than those for the other two stages, suggesting that the boundary effect became more obvious with increasing reaction time. With less residual Cr(VI) in solution and fewer adsorption sites on the surface, the intraparticle

diffusion rate decreased; thus, the reaction gradually reached equilibrium. The *C* value increased with increasing initial concentration of Cr(VI), which indicated that adsorption played an important role in the removal process. Moreover, intraparticle diffusion was not the only mechanism operating in the process because all of *C* were not the origin.

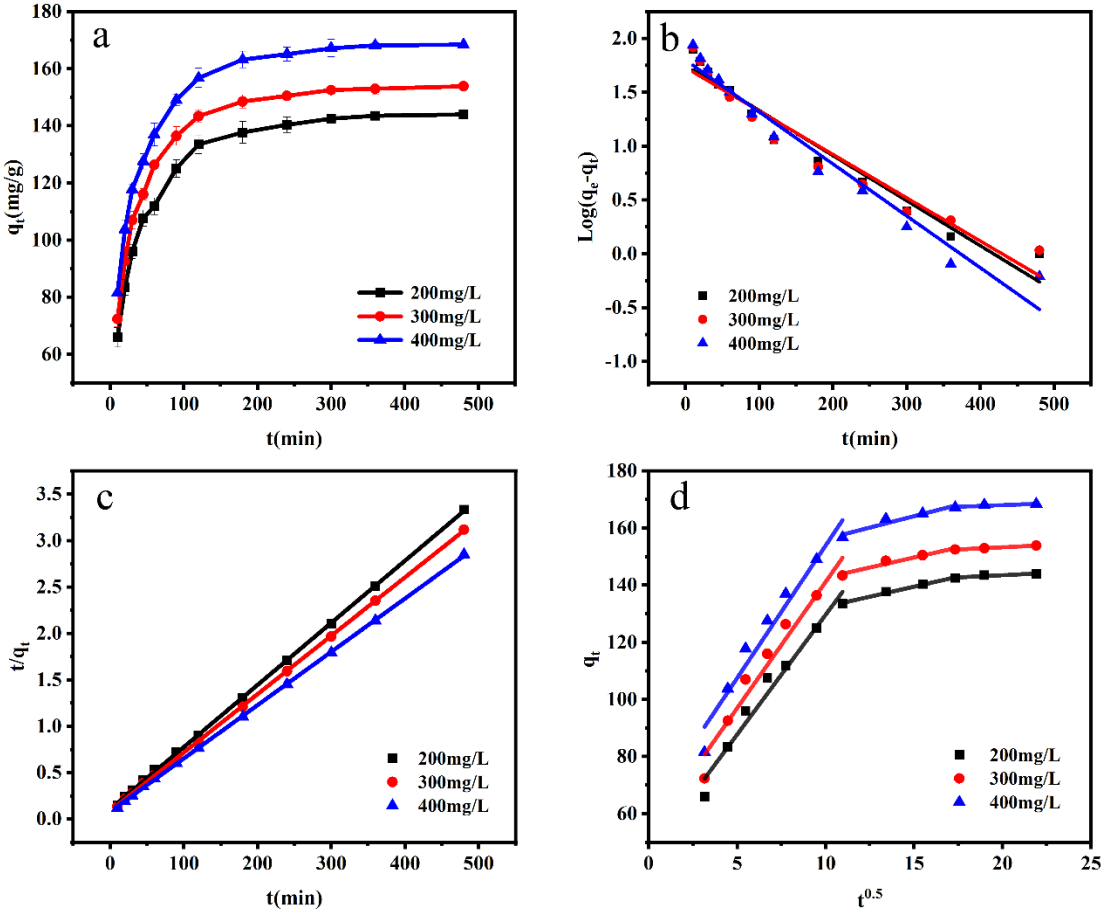

Fig. 3 Kinetic analyses for adsorption of Cr(VI) by SC@ZVI@CS-AA: (a) Effect of contact time on the capacity for Cr(VI) adsorption by SC@ZVI@CS-AA (adsorbent dosage = 0.8 g/L, pH = 3, and T = 25°C); (b) Fit of the pseudo first-order model for adsorption of Cr(VI) by SC@ZVI@CS-AA; (c) Fit of the pseudo second-order model for adsorption of Cr(VI) by SC@ZVI@CS-AA; and (d) Fit of the intraparticle diffusion model for adsorption of Cr(VI) by SC@ZVI@CS-AA

Adsorption isotherms

The effect of the initial Cr(VI) concentration on adsorption at 25°C is shown in Fig. 4a. The capacity for adsorption of Cr(VI) increased gradually with increasing initial concentration. The adsorption capacity increased rapidly below 100 mg/L but slowly within the range 100 mg/L to 500 mg/L. Conversely, the overall removal efficiency showed a downward trend. Since the adsorbent dosage was fixed, the number of adsorption-reduction sites on the surface was basically the same. In this case, SC@ZVI@CS-AA was not fully involved in the reaction at low concentrations of Cr(VI). The higher the concentration of Cr(VI) in the solution was, the more chromium-containing anions, which enhanced chemical adsorption of Cr(VI) by functional groups ($–NH_2$, –OH and $–SO_3H$). In addition, redox reactions occurred when Cr(VI) and ZVI levels were increased, further improving the utilization rate of the adsorbent. The slow growth trend for adsorption capacities with initial concentrations between 100 and 500 mg/L was due to the limited number of groups carried by the material itself. At the same time, when the Cr(VI) concentration was high, a substantial amount of Cr(VI) was reduced to Cr(III), which increased the amount of Cr(III)-Fe(III) hydroxyl oxide bound with ZVI and formed a passivation layer comprising $Cr_{0.667}Fe_{0..333}OOH$ or $Cr_{0.667}Fe_{0.333}(OH)_3$(Powell et al., 1995). This passivation layer prevented the iron core from transferring electrons. Although the removal efficiency of Cr(VI) decreased, the adsorption capacity increased.

Langmuir, Freundlich and Tempkin isotherm models for the adsorption of Cr(VI)

are displayed in Fig. 4b, c and d, respectively, and the related coefficients are listed in Table S3. As the results illustrate, the R^2 value for the Langmuir model was much closer to 1.0 and higher than those of the Freundlich and Tempkin models, demonstrating that the Langmuir model was more suited for fitting the data for adsorption of Cr(VI) by SC@ZVI@CS-AA. Therefore, the adsorption process likely involved monolayer adsorption, and the maximum capacity for adsorption of Cr(VI) by SC@ZVI@CS-AA increased with increasing temperature. It is generally believed that an empirical constant of the Freundlich isotherm ($1/n$) less than 1 is more conducive to adsorption(A et al., 2012). The $1/n$ value of this experiment was between 0.08 and 0.01, indicating that Cr(VI) was easily adsorbed by the adsorbent. Based on the equilibrium binding constant (K_T), SC@ZVI@CS-AA had a large equilibrium binding energy for removal of Cr(VI), suggesting that a strong chemical reaction occurred during the adsorption process.

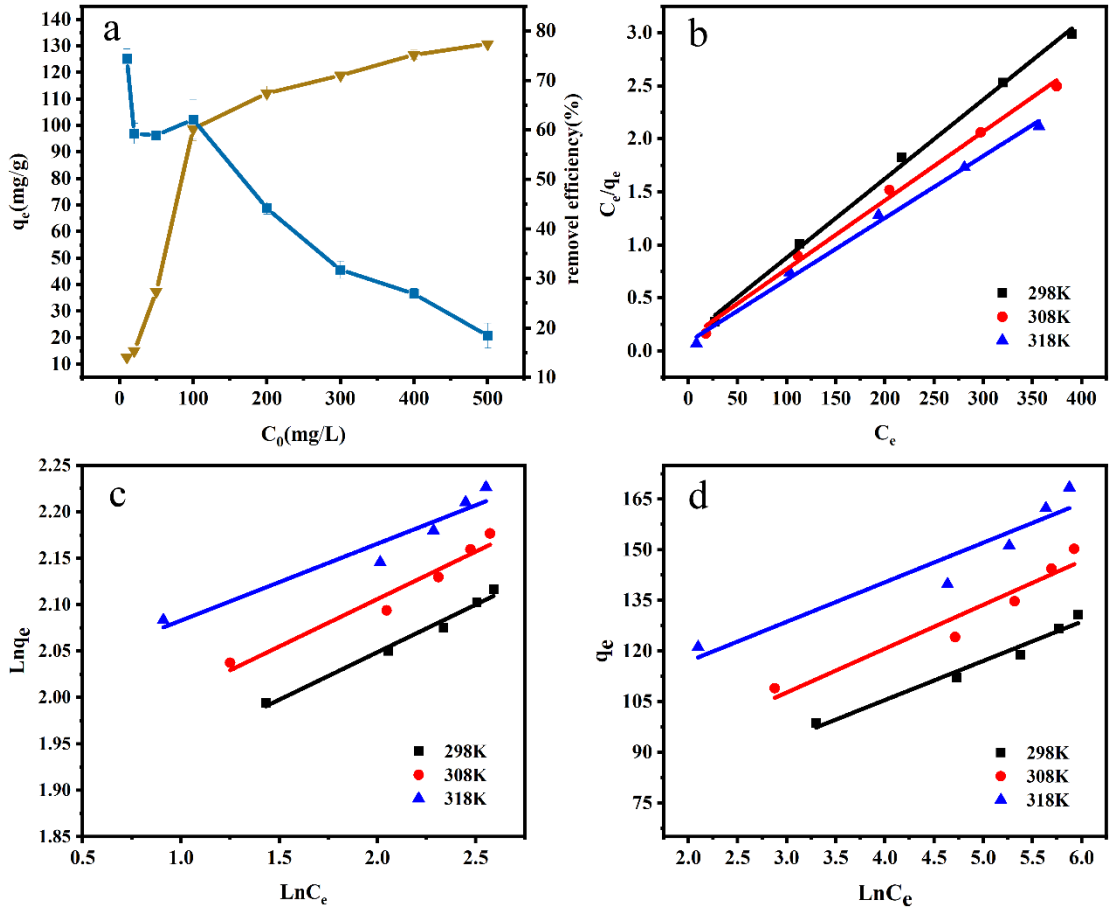

Fig. 4 Isotherms for adsorption of Cr(VI) by SC@ZVI@CS-AA: (a) Effect of the initial Cr(VI) concentration on the removal efficiency and capacity for adsorption of Cr(VI) by SC@ZVI@CS-AA (t = 12 h, adsorbent dosage = 0.8 g/L, pH = 3, and T = 25°C); (b) Langmuir isotherm curve for SC@ZVI@CS-AA; (c) Freundlich isotherm curve for SC@ZVI@CS-AA; and (d) Temkin isotherm model curve for SC@ZVI@CS-AA

Effect of various composite ratios of SC@ZVI@CS-AA

The effect of different compounding ratios on the adsorption of Cr(VI) is shown in Fig. 5. Fig. 5a shows that when the ratio of SC to CS reached 2 to 1, the adsorption capacity for Cr(VI) was the largest (54.5 mg/g). When this ratio was higher, the amount of CS loaded on SC was insufficient and there were not enough functional groups

455 (−NH_2 and −OH) undergoing reactions with Cr(VI), which limited the adsorption of
456 Cr(VI). Moreover, CS could not stabilize ZVI due to the low CS content, which allowed
457 ZVI agglomeration(He et al., 2007; Bhatia and Ravi, 2003). When the ratio of the two
458 was lower, the amount of CS present was so high that polymeric CS-AA formed on the
459 surface of SC, reducing the porosity of the material and limiting contact between ZVI
460 and Cr(VI) or Cr(III).

461 As shown in Fig. 5b, when the SC:ZVI mass ratio was 3 to 1, the adsorption
462 capacity for Cr(VI) reached the highest value (142.42 mg/g). When the amount of ZVI
463 loaded on SC was too high, the adsorption sites of SC were easily saturated. The more
464 ultrafine iron powder there was, the more likely it was to form clusters. Appropriately
465 reducing the load of ZVI was more conducive to uniform dispersion, thereby allowing
466 ZVI to serve as a reductant.

467 **Effect of pH**

468 The effect of initial pH on chromium removal is shown in Fig. 5c. pH had an
469 important influence on the adsorption results. The removal efficiency decreased from
470 59.30% to 2.60% when the pH was increased from 3 to 8.5, and the capacity for
471 adsorption of Cr(VI) by SC@ZVI@CS-AA decreased from 134.37 mg/g to 6.37 mg/g.
472 Farther, the removal capacity of Total Cr by SC@ZVI@CS-AA decreased from 119.30
473 mg/g to 9.86 mg/g with pH increasing from 3 to 8.5. It is obvious that removal capacity
474 of Cr(VI) is higher than that of Total Cr. It may be because SC@ZVI@CS-AA reduced
475 a part of Cr(VI) to Cr(III), which leaded to Cr(VI) concentration lower than Total Cr in

476 the solution, so the adsorption capacity of Cr(VI) was higher.

477 Geng et al.(Bing et al., 2009) investigated the effect of pH on the stability of ZVI
478 loaded onto CS. Strong acid or strong alkali had an important impact on the adsorption,
479 and relatively high removal rates were observed under acidic conditions. This was
480 mainly related to the presence of Cr(VI) in solution and the charge on the adsorbent
481 surface. $HCrO_4^-$、$Cr_2O_7^{2-}$ and CrO_4^{2-} are the main forms of Cr(VI) present in aqueous
482 environments(Araghi et al., 2015). When the pH was between 1 and 6.8, Cr(VI) existed
483 mainly as $HCrO_4^-$ and $Cr_2O_7^{2-}$. When the pH was higher than 6.8, it existed mainly in
484 the form of $Cr_2O_4^{2-}$ (Gan et al., 2015). $HCrO_4^-$ and $Cr_2O_7^{2-}$ are easily reduced(Zhou et
485 al., 2016), which would increase the capacity of the adsorbent to reduce Cr(VI). In
486 addition, compared with $Cr_2O_4^{2-}$, the lower adsorption free energy for $HCrO_4^-$
487 facilitated adsorption.

488 On the other hand, the functional groups ($-OH$, $-NH_2$ and $-SO_3H$) on
489 SC@ZVI@CS-AA would undergo protonation ($-OH^+$, $-NH_2^+$ and $-SO_3H^+$) in an
490 acidic environment, which would enhance the electrostatic attraction between
491 SC@ZVI@CS-AA and $HCrO_4^-$ or $Cr_2O_7^{2-}$ (Fonseca et al., 2009; Zhang et al., 2012;
492 Wasim et al., 2015). Therefore, SCZVI@CS-AA showed a better efficiency for removal
493 of Cr(VI) under acidic conditions.

494 **Effect of temperature**

495 The effects of temperature on chromium removal with different initial

concentrations (100, 200, 300, 400 and 500 mg/L) are shown in Fig. 5d. At certain Cr(VI) concentrations, the adsorption capacities of Cr(VI) and Total Cr both increased with increasing temperature. As the reaction temperature increased, the reactivities of functional groups ($-NH_2$, $-OH$, and $-SO_3H$) present on the adsorbent surface were enhanced, which increased the rate of metal ions passing through the boundary layer and pore channels of SC and further enhanced adsorption and reduction.

Based on the equilibrium values obtained for adsorption with different initial Cr(VI) concentrations at different temperatures, thermodynamic parameters were calculated. The ΔH^{θ} (12.30 KJ/mol) for the adsorption process was positive, indicating that adsorption of Cr(VI) by SC@ZVI@CS-AA was endothermic. The ΔH^{θ} data were used to illustrate that rising temperatures enhance Cr(VI) adsorption. The ΔS^{θ} (41.08 KJ/mol) confirmed that the disorder of the solid-liquid interface increased during adsorption(Tan et al., 2009), which was conducive to adsorption(Zhang et al., 2010). The value of ΔG^{θ} (0.06 KJ/mol) decreased with increasing temperature and was negative above 35°C, indicating that the adsorption process was spontaneous when the temperature was higher than 35°C.

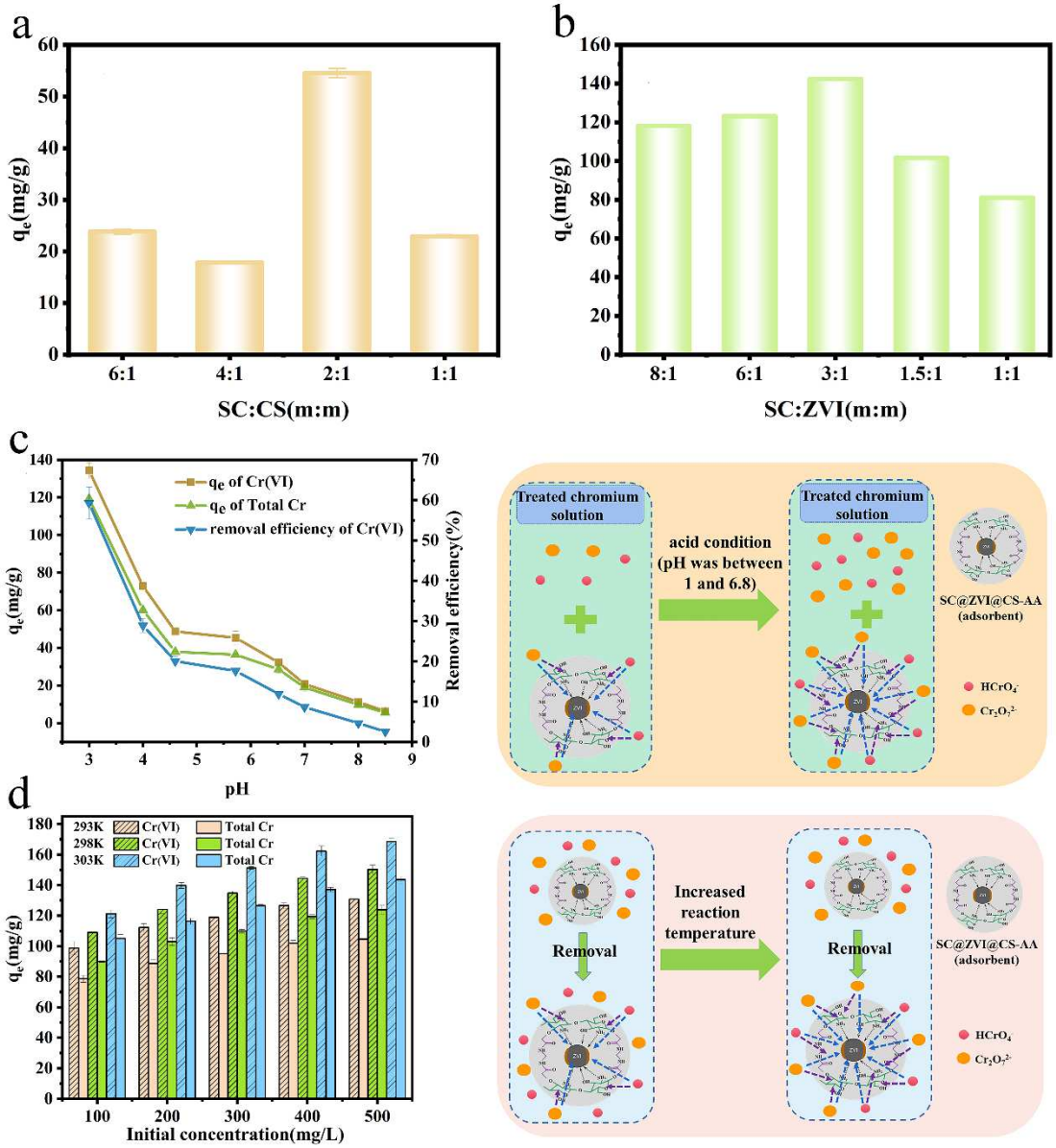

512

513 **Fig. 5** Effect of various composite ratios, pH and coexisting ions on chromium removal: (a) Effect

514 of SC:CS (m:m); (b) Effect of SC:ZVI (m:m) (C_0 = 200 mg/L, pH = 3, t = 5 h, and T = 25°C). (c)

515 Effect of pH (C_0 = 200 mg/L; adsorbent dosage = 0.8 g/L, t = 5 h, and T = 25°C); (d) Effect of

516 temperature (t = 12 h, C_0 = 200 mg/L, adsorbent dosage = 0.8 g/L, and pH = 3)

517 **Effect of SC@ZVI@CS-AA dosage**

518 The effect of SC@ZVI@CS-AA dosage on chromium removal is shown in Fig.

519 6a. With increasing SC@ZVI@CS-AA dosage, the capacity for adsorption of Cr(VI)
520 and showed an overall downward trend, which was higher than the adsorption capacity
521 of Total Cr. The adsorption capacity of Cr(VI) reached a maximum value (119.39 mg/g)
522 at a dose of 0.8 g/L and then began to decrease. The removal efficiency for Cr(VI)
523 showed an upward trend; moreover, it increased slowly with increasing dosage.

524 With increasing adsorbent dosage, the effect of more ZVI reductant on Cr(VI) was
525 enhanced. At the same time, the number of active sites on the surface increased
526 significantly, which improved mass transfer between the SC@ZVI@CS-AA and
527 chromium-containing anions, increased the collision frequencies of chromium
528 particles(Chen et al., 2012), and further enhanced adsorption. However, due to the
529 constant concentration of Cr(VI) in the solution, excess reaction sites provided by
530 SC@ZVI@CS-AA did not participate in the reaction. Therefore, the chromium
531 adsorption capacity per unit mass of SC@ZVI@CS-AA was decreased due to the
532 reduced utilization of SC@ZVI@CS-AA.

533 **Effect of coexisting ions**

534 Other anions and cations coexisting with Cr(VI) are often present in groundwater,
535 which causes varying degrees of interference in mass transfers between SC@ZVI@CS-
536 AA and chromium-containing anions(Cao et al., 2017). The effects of interfering ions
537 on chromium removal are shown in Fig. 6b. After addition of different interfering ions
538 (Ca^{2+}, Mg^{2+}, Cd^{2+}, Na^{+}, Cl^{-}, NO_3^{-}, SO_4^{2-} and $H_2PO_4^{2-}$), the capacities for adsorption of
539 Cr(VI) and Total Cr changed differently. The inhibition by SO_4^{2-} was the most

significant, resulting in a 58.35% and 58.06% descent in Cr(VI) and Total Cr removal compared with the blank sample, respectively. On the one hand, binding between SO_4^{2-} and $-NH_2$ led to competitive adsorption with chromium-containing anions. On the other hand, the distribution of charges around the occupied adsorption sites caused by SO_4^{2-} weakened the electrostatic attractions between SC@ZVI@CS-AA and chromate(Mohan and Pittman, 2006). Wang et al.(Wang et al., 2018) also found that a variety of interfering ions exhibited effects on the adsorption process of PPy-Fe_3O_4/rGO, and the inhibitory effect of SO_4^{2-} was the most significant. When SO_4^{2-} concentration increased from 0 to 0.1 g/L, the removal efficiency decreased by 44.4% .

Cyclic adsorption by SC@ZVI@CS-AA

The experimental results for cyclic adsorption are shown in Fig. 6. As Fig. 6c shows, when SC@ZVI@CS-AA was recycled three times, the maximum decrease in Cr(VI) adsorption capacity was 4.56 mg/g, and the maximum decrease in total Cr(VI) adsorption capacity was 19.01 mg/g. When sodium hydroxide (NaOH) was used for desorption, part of the Cr(VI) did not elute from SC@ZVI@CS-AA, which reduced the number of sites available during reuse. As shown in Fig. 6d, the desorption efficiency decreased from 89.68% to 87.13% for the second cycle of SC@ZVI@CS-AA. This showed that NaOH was better for desorption of Cr(VI). The higher desorption rate was more conducive to reuse of SC@ZVI@CS-AA and recovery of heavy metals. This result also indicated that ion exchange and coordination occurred during the removal of

Cr(VI). All of the above results illustrated that SC@ZVI@CS-AA realized cyclic adsorption of Cr(VI).

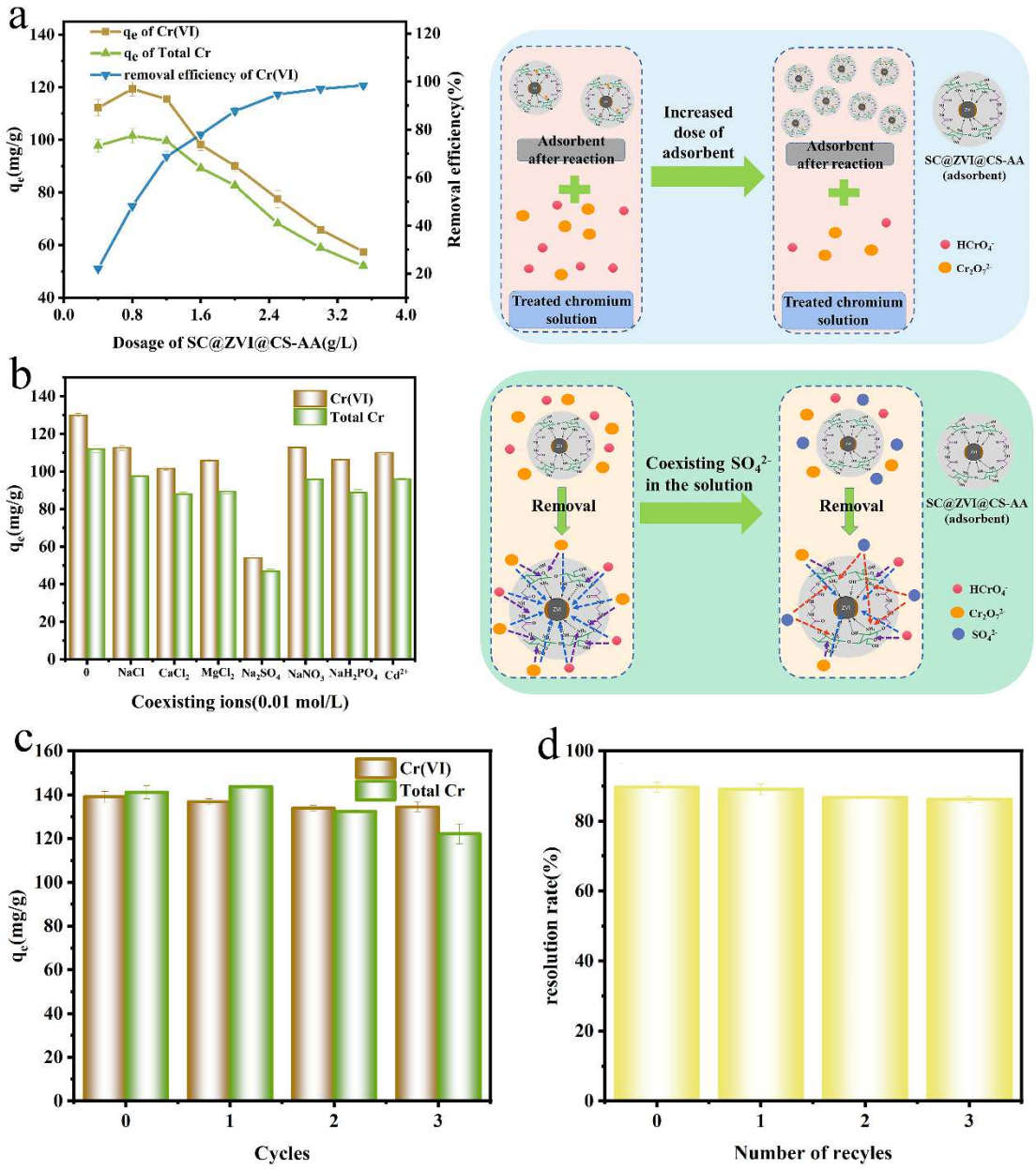

Fig. 6 Effect of adsorbent dosage and coexisting ions on chromium removal and cyclic adsorption performance of SC@ZVI@CS-AA: (a) Effect of adsorbent dosage (C_0 = 200 mg/L, pH = 3, t = 5 h, and T = 25°C); (b) Effect of coexisting ions (C_0 = 200 mg/L, adsorbent dosage = 0.8 g/L,pH =

3, t = 5 h, and T = 25°C); (c) Capacities for Cr(VI) and Total Cr adsorption by SC@ZVI@CS-AA with increasing cycles; (d) Efficiency of Cr(VI) desorption from SC@ZVI@CS-AA with increasing cycles(C_0 = 200 mg/L, adsorbent dosage = 0.8 g/L, pH = 3, t = 5 h, and T = 25°C)

Mechanisms of Cr(VI) removal by SC@ZVI@CS-AA

In summary, the mechanism of action between SC@ZVI@CS-AA and Cr(VI) is thought to be as shown in Fig. 7. ZVI reduces Cr(VI) to produce Fe(III) and Cr(III). The two form coprecipitated species ($Fe_xCr_{1-x}OOH$ and $Fe_xCr_{1-x}(OH)_3$) on the surface of ZVI at a high pH, which hinders electron transfer between ZVI and Cr(VI) and reduces reaction activity.

The CS modified by AA contains a large number of $-NH_2$ and $-OH$ groups. They combine with some of the Fe(III) to form a stable complex, thereby inhibiting the formation of a passivation layer on the surface of ZVI so that reduction of Cr(VI) by ZVI is promoted. Moreover, the functional groups ($-OH$, $-NH_2$ and $-SO_3H$) carried by SC@ZVI@CS-AA undergo protonation ($-OH^+$, $-NH_2^+$ and $-SO_3H^+$) under acidic conditions, making the surface of SC@ZVI@CS-AA positively charged. Under the same conditions, Cr(VI) exists as $HCrO_4^-$ and $Cr_2O_7^{2-}$. The combination of SC@ZVI@CS-AA and Cr(VI) results from electrostatic attraction.

The sulfonated coal formed by acid treatment plays a role in supporting the ZVI modified by CS-AA. At the same time, the number of reactive pores and specific surface area are increased, and $-SO_3H$ on the surface is activated to form $-SO_3H^+$, which aids adsorption of Cr(VI).

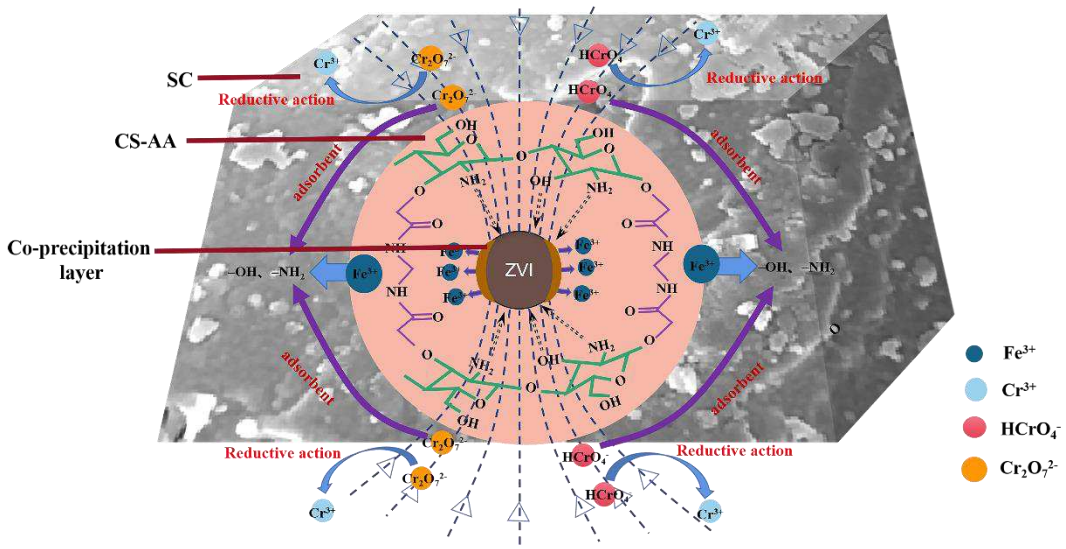

Fig. 7 Mechanisms of Cr(VI) removal by SC@ZVI@CS-AA

Conclusion

(1) ZVI was stabilized by CS-AA sol, and SC was used as a carrier to prepare SC@ZVI@CS-AA. Characterization showed that the surface of SC@ZVI@CS-AA exhibited a cross-linked network structure rich in amino and hydroxyl groups and showed good thermal stability.

(2) The pseudo second-order model gave the best fit for the rate of Cr(VI) adsorption by the SC@ZVI@CS-AA composite, indicating that chemisorption occurred during the process. The Langmuir isotherm model was best suited for describing the adsorption process. Thermodynamic studies indicated that the adsorption of Cr(VI) was spontaneous when the temperature was above 35°C.

(3) Under the optimal conditions, the efficiency for removal of Cr(VI) by SC@ZVI@CS-AA was as high as 98.5%. The capacity for adsorption of Cr(VI) was still maintained above 70% after three reuses, indicating good cyclic adsorption of

Cr(VI) on SC@ZVI@CS-AA. In particular, SO_4^{2-} in the solution inhibited the removal of Cr(VI) significantly.

(4) In an acidic environment, SC@ZVI@CS-AA showed good removal of adsorbed Cr(VI). SC@ZVI@CS-AA exhibited cyclic adsorption and prospects for application. However, this experiment only explored the influences of the main environmental factors on the removal of Cr(VI) by SC@ZVI@CS-AA. The actual situation for chromium pollution in groundwater would be more complex. According to the specific application, the influence of the permeability coefficients of materials, water flow rate and service lives of materials should be considered fully.

Authors' contributions This idea was given by Jianlei Gao. Mengyuan Feng analyzed the data and wrote the paper. Mengyuan Feng, Yixin Yan, Zixu Zhao and Yingchun Wang proofread the paper. All authors read and approved the final manuscript.

Funding This work was supported by a project of the Department of Science and Technology of Henan Province (project number 182102210194)

Data availability All data and models that support the fundings of this study are available from the corresponding author upon reasonable request.

Declarations

Ethics approval Study did not use any data which need approval.

Consent to participate All authors have participated in the process, read and agreed to the published version of the manuscript.

623 **Competing interests** The authors declare that they have no competing interests.

624 ## References

625 A, C.Y.H., B, S.L. Lo, C, Y.H.L., B, Y.W.H., D, K.S., E, C.J.L., 2010. Hexavalent
626 chromium removal from near natural water by copper–iron bimetallic particles.
627 Water Res. 44, 3101–3108.

628 A, X.M., A, G.H., A, W.X., B, W.W., A, Y.L., A, J.G., 2012. Preparation of graphene
629 oxide aerogel and its adsorption for Cu2+ ions - ScienceDirect. Carbon N. Y. 50,
630 4856–4864.

631 Akg, A., Mg, B., 2005. Synthesis and surface engineering of iron oxide nanoparticles
632 for biomedical applications - ScienceDirect. Biomaterials 26, 3995–4021.

633 Aksu, Z., 2002. Determination of the equilibrium, kinetic and thermodynamic
634 parameters of the batch biosorption of nickel(II) ions onto Chlorella vulgaris.
635 Process Biochem. 38, 89–99.

636 Araghi, S.H., Entezari, M.H., Chamsaz, M., 2015. Modification of mesoporous silica
637 magnetite nanoparticles by 3-aminopropyltriethoxysilane for the removal of
638 Cr(VI) from aqueous solution. Microporous Mesoporous Mater.

639 Araújo, C.S.T., Almeida, I., Rezende, H.C., Marcionilio, S., Léon, J.J.L., Matos, T.
640 De, 2017. Elucidation of mechanism involved in adsorption of Pb(II) onto
641 lobeira fruit (Solanum lycocarpum) using Langmuir, Freundlich and Temkin
642 isotherms. Microchem. J. 137, 348–354.

643 B, F.Z.A., A, E.R., B, D.Y., A, M.E.T.S., 2013. Adsorption of Cd(II) and Pb(II) by a

644 novel EGTA-modified chitosan material: Kinetics and isotherms. J Colloid
645 Interface 409, 174–182.
646 Belhaj, E., Lafhaj, Z., Zakaria, K., Depelsenaire, G., 2015. Formulation of a
647 Permeable Reactive Mixture for Groundwater Remediation Based on an
648 Industrial Co-product: Permeability and Copper Retention Study. Waste &
649 Biomass Valorization 6, 263–272.
650 Bhatia, S.C., Ravi, N., 2003. A Mössbauer study of the interaction of chitosan and D-
651 glucosamine with iron and its relevance to other metalloenzymes.
652 Biomacromolecules 4, 723.
653 Bing, G., Jin, Z., Li, T., Qi, X., 2009. Preparation of chitosan-stabilized Fe0
654 nanoparticles for removal of hexavalent chromium in water. Sci. Total Environ.
655 407, 4994–5000.
656 Bronstein, K., 2005. Permeable Reactive Barriers for Inorganic and Radionuclide
657 Contamination. Environ. Prot. Agency.
658 Cao, W., Wang, Z., Ao, H., Yuan, B., 2017. Removal of Cr(VI) by corn stalk based
659 anion exchanger: the extent and rate of Cr(VI) reduction as side reaction.
660 Colloids Surfaces A Physicochem. Eng. Asp. 539, 424–432.
661 Chen, A., Zeng, G., Chen, G., Hu, X., Ming, Y., Song, G., Shang, C., Lu, L., Zou, Z.,
662 Xie, G., 2012. Novel thiourea-modified magnetic ion-imprinted chitosan/TiO2
663 composite for simultaneous removal of cadmium and 2,4-dichlorophenol. Chem.
664 Eng. J. 191, 85–94.

665 Chen, K., Jiang, S., Reincke, F., Tong, W., Wang, D., Gao, C., 2006. Chitosan-
666 mediated synthesis of gold nanoparticles on patterned poly(dimethylsiloxane)
667 surfaces. Biomacromolecules 7, 1203–1209.
668 Chen, Y., Mohanraj, V.J., Parkin, J.E., 2003. Chitosan-dextran Sulfate Nanoparticles
669 for Delivery of an Anti-angiogenesis Peptide. Lett. Pept. Sci. 10, 621–629.
670 Divya, Chauhan, and, Nalini, Sankararamakrishnan, 2008. Highly enhanced
671 adsorption for decontamination of lead ions from battery wastewaters using
672 chitosan functionalized with xanthate. Bioresour. Technol. 99, 9021–9024.
673 Espinoza-Sánchez, M.A., Arévalo-Nio, K., Quintero-Zapata, I., Castro-González, I.,
674 Almaguer-Cantú, V., 2019. Cr(VI) adsorption from aqueous solution by fungal
675 bioremediation based using Rhizopus sp. J. Environ. Manage. 251, 109595-.
676 Fonseca, B., Maio, H., Quintelas, C., Teixeira, A., Tavares, T., 2009. Retention of Cr
677 (VI) and Pb (II) on a loamy sand soil:: Kinetics, equilibria and breakthrough.
678 Chem. Eng. J. 152, 212–219.
679 Gan, C., Liu, Y., Tan, X., Wang, S., Zeng, G., Zheng, B., Li, T., Jiang, Z., Liu, W.,
680 2015. Effect of porous zinc–biochar nanocomposites on Cr(VI) adsorption from
681 aqueous solution. RSC Adv. 5.
682 Gong, Y., Tang, J., Zhao, D., 2016. Application of iron sulfide particles for
683 groundwater and soil remediation: A review. Water Res. 89, 309–320.
684 Guan, Q., Li, F., Chen, X., Tian, C., Liu, C., Liu, D., 2019. Assessment of the use of a
685 zero-valent iron permeable reactive barrier for nitrate removal from groundwater

686 in the alluvial plain of the Dagu River, China. Environ. Earth Sci. 78, 1–12.
687 Guibal, E., 2004. Interactions of metal ions with chitosan-based sorbents: a review.
688 Sep. Purif. Technol. 38, 43–74.
689 Hadi, P., Barford, J., Mckay, G., 2013. Toxic heavy metal capture using a novel
690 electronic waste-based material-mechanism, modeling and comparison. Environ.
691 Sci. Technol. 47, 8248–8255.
692 Hameed, B.H., Din, A.T.M., Ahmad, A.L., 2007. Adsorption of methylene blue onto
693 bamboo-based activated carbon: kinetics and equilibrium studies. J. Hazard.
694 Mater. 141, 819–825.
695 He, F., Zhao, D., Liu, J., Roberts, C.B., 2007. Stabilization of FePd Nanoparticles
696 with Sodium Carboxymethyl Cellulose for Enhanced Transport and
697 Dechlorination of Trichloroethylene in Soil and Groundwater. Ind. Eng. Chem.
698 Res. 46, 29–34.
699 Hedin, R.S., Watzlaf, G.R., Nairn, R.W., 1994. Passive Treatment of Acid Mine
700 Drainage with Limestone. J. Environ. Qual. 23(6), 1338–1345.
701 Henderson, A.D., Demond, A.H., 2007. Long-term performance of zero-valent iron
702 permeable reactive barriers: A critical review. Environ. Eng. Sci.
703 https://doi.org/10.1089/ees.2006.0071
704 Hu, X.J., Wang, J.S., Liu, Y.G., Li, X., Zeng, G.M., Bao, Z.L., Zeng, X.X., Chen,
705 A.W., Long, F., 2011. Adsorption of chromium (VI) by ethylenediamine-
706 modified cross-linked magnetic chitosan resin: Isotherms, kinetics and

thermodynamics. J. Hazard. Mater. 185(1), 306–314.

Jamil, F., Al-Muhtaseb, A.H., Naushad, M., Baawain, M., Viswanadham, N., 2017. Evaluation of synthesized green carbon catalyst from waste date pits for tertiary butylation of phenol. Arab. J. Chem. 13.

Jin, Q., Zhang, S., Tao, W., Jian, W., Gu, P., Zhao, G., Wang, X., Chen, Z., Tasawar, H., Wang, X., 2018. Simultaneous adsorption and oxidative degradation of Bisphenol A by zero-valent iron/iron carbide nanoparticles encapsulated in N-doped carbon matrix. Environ. Pollut. 243, 218–227.

Jobby, R., Jha, P., Yadav, A.K., Desai, N., 2018. Biosorption and biotransformation of hexavalent chromium [Cr(VI)]: A comprehensive review. Chemosphere 207, 255–266.

Lei, C., Wang, C., Chen, W., He, M., Huang, B., 2020. Polyaniline@ magnetic chitosan nanomaterials for highly efficient simultaneous adsorption and in-situ chemical reduction of hexavalent chromium: Removal efficacy and mechanisms. Sci. Total Environ. 733, 139316.

Lu. X. F., 2019. Application of Modified Chitosan in Removal of Heavy Metals from Water, Chengdu University of technol. 05.

Lei, Z., Zeng, Y., Cheng, Z., 2016. Removal of heavy metal ions using chitosan and modified chitosan: A review. J. Mol. Liq. 214, 175–191.

Liu, Y., Mou, H., Chen, L., Mirza, Z.A., Liu, L., 2015. Cr(VI)-contaminated groundwater remediation with simulated permeable reactive barrier (PRB) filled

728 with natural pyrite as reactive material: Environmental factors and effectiveness.
729 J. Hazard. Mater. 298, 83–90.
730 Lu, M., Zhang, Y.M., Guan, X.H., Xu, X.H., Gao, T.T., 2014. Thermodynamics and
731 kinetics of adsorption for heavy metal ions from aqueous solutions onto surface
732 amino-bacterial cellulose. Trans. Nonferrous Met. Soc. China 24, 1912–1917.
733 Mei, J., Zhang, H., Li, Z., Ou, H., 2019. J. Ground Water. A novel
734 tetraethylenepentamine crosslinked chitosan oligosaccharide hydrogel for total
735 adsorption of Cr(VI). Carbohydr. Polym. 224, 115154-.
736 Mohan, D., Pittman, C.U., 2006. Activated carbons and low cost adsorbents for
737 remediation of tri- and hexavalent chromium from water. J. Hazard. Mater. 137,
738 762–811.
739 Ni, X, Z., 1997. The basic research of preparing activated sulphonated coal, Shandong
740 Institute of mining and Technology, 020, 66–70.
741 Neto, J. de O.M., Bellato, C.R., de Castro Silva, D., 2019. Iron oxide/carbon
742 nanotubes/chitosan magnetic composite film for chromium species removal.
743 Chemosphere 218, 391–401.
744 Obiri-Nyarko, F., Grajales-Mesa, S.J., Malina, G., 2014. An overview of permeable
745 reactive barriers for in situ sustainable groundwater remediation. Chemosphere
746 111, 243–259.
747 Pbv, A., Cam, A., Ad, A., Vab, A., Atpa, B., 2011. Polyacrylic acid-based and
748 chitosan-based hydrogels for adsorption of cadmium: Equilibrium isotherm,

749 kinetic and thermodynamic studies. J. Environ. Chem. Eng. 7, 103327.
750 Pourcq, K. De, Ayora, C., Garcia-Gutierrez, M., Missana, T., Carrera, J., 2015. A clay
751 permeable reactive barrier to remove Cs-137 from groundwater: Column
752 experiments. J. Environ. Radioact. 149, 36–42.
753 Powell, R.M., Puls, R.W., Hightower, S.K., Sabatini, D.A., 1995. Coupled iron
754 corrosion and chromate reduction: mechanisms for subsurface remediation.
755 Environ. Sci. Technol. 29, 1913–1922.
756 Tan, I., Ahmad, A.L., Hameed, B.H., 2009. Adsorption isotherms, kinetics,
757 thermodynamics and desorption studies of 2,4,6-trichlorophenol on oil palm
758 empty fruit bunch-based activated carbon. J. Hazard. Mater. 164, 473–482.
759 Tao, S., Xu, P., Liu, Q., Jian, X., Xie, W., 2003. Graft polymerization of methacrylic
760 acid onto carboxymethyl chitosan. Eur. Polym. J. 39, 189–192.
761 Tasharrofi, S., Rouzitalab, Z., Maklavany, D.M., Esmaeili, A., Taghdisian, H., 2020.
762 Adsorption of cadmium using modified zeolite-supported nanoscale zero-valent
763 iron composites as a reactive material for PRBs. Sci. Total Environ. 736,
764 139570.
765 Water quality—Determination of chromium(VI) —1,5 Diphenylcarbohydrazide
766 spectrophotometric method, GB/T 7467–1987.
767 Wu, G., 2002. Characterization and Application of Material Structure.
768 Wang, Jim, J., Zhang, Zengqiang, Ali, Amjad, Li, Ronghua, Manlin, 2016. Removal
769 of Pb(II) and Cd(II) ions from aqueous solution by thiosemicarbazide modified

chitosan. Int. J. Biol. Macromol. Struct. Funct. Interact. 86, 876–884.

Wang, R.Y., Zhang, W., Zhang, L.Y., Hua, T., Zuo, Q.T., 2019. Polyacrylic acid-based and chitosan-based hydrogels for adsorption of cadmium: Equilibrium isotherm, kinetic and thermodynamic studies,Adsorption characteristics of Cu(II) and Zn(II) by nano-alumina material synthesized by the sol-gel method in batch mode. Environ. Sci. Pollut. Res. 26.

Wang, S., Li, X., Liu, Y., Zhang, C., Tan, X., Zeng, G., Song, B., Jiang, L., 2018. Nitrogen-containing amino compounds functionalized graphene oxide: Synthesis, characterization and application for the removal of pollutants from wastewater: A review. J. Hazard. Mater. 342, 177–191.

Wasim, A.S., Latif, M.M., Bhatti, T.M., Kashif, N., Muhammad, I.D., 2015. Dispersion of Iron Nanoparticles by Polymer-Based Hybrid Material for Reduction of Hexavalent Chromium. J. Nanomater. 2015, 1–8.

Wilkin, R.T., Puls, R.W., Sewell, G.W., 2010. Long-term performance of permeable reactive barriers using zero-valent iron: geochemical and microbiological effects. Ground Water 41, 493–503.

Wu, F.C., Tseng, R.L., Juang, R.S., 2001. Enhanced abilities of highly swollen chitosan beads for color removal and tyrosinase immobilization. J. Hazard. Mater. 81, 167–177.

Zhan, H, J., Wu. Z. Q, Zhang. T. F., Bi. S. X., Liu. W. Y., 2017. Preparation of sulfonated Taixi coal adsorbent and adsorption study, School of Chem. Eng. of

Ningxia University, 46.

Zhang, R., Ma, H., Wang, B., 2010. Removal of Chromium(VI) from Aqueous Solutions Using Polyaniline Doped with Sulfuric Acid. Ind. Eng. Chem. Res. 49, 9998–10004.

Zhang, Y., Li, Y., Li, J., Sheng, G., Zheng, X., 2012. Enhanced Cr(VI) removal by using the mixture of pillared bentonite and zero-valent iron. Chem. Eng. J. s 185–186, 243–249.

Zhao, D., Sheng, G., Hu, J., Chen, C., Wang], X., 2011. The adsorption of Pb(II) on Mg2Al layered double hydroxide. Chem. Eng. J. 03, 082.

Zhiya, Ma, Huizhou, Liu, Laboratory, of, Separation, Science, and, Engineering, 2007. Synthesis and surface modification of magnetic particles for application in biotechnology and biomedicine. China Particuology Z1, 13–22.

Zhou, L., Liu, Y., Liu, S., Yin, Y., Zeng, G., Tan, X., Hu, X., Hu, X., Jiang, L., Ding, Y., 2016. Investigation of the adsorption-reduction mechanisms of hexavalent chromium by ramie biochars of different pyrolytic temperatures. Bioresour. Technol. 218, 351–359.

Supplementary Files

This is a list of supplementary files associated with this preprint. Click to download.

- SupplementaryMaterial.docx